Two-dimensional optical three-pulse photon echo spectroscopy. II. Signatures of coherent electronic motion and exciton population transfer in dimer two-dimensional spectra

Andrei V. Pisliakov, Tomáš Manal, and Graham R. Fleming

Citation: The Journal of Chemical Physics **124**, 234505 (2006); doi: 10.1063/1.2200705
View online: http://dx.doi.org/10.1063/1.2200705
View Table of Contents: http://scitation.aip.org/content/aip/journal/jcp/124/23?ver=pdfcov
Published by the AIP Publishing

Two-dimensional optical three-pulse photon echo spectroscopy. II. Signatures of coherent electronic motion and exciton population transfer in dimer two-dimensional spectra

Andrei V. Pisliakov, Tomáš Mančal, and Graham R. Fleming[a)]
Department of Chemistry, University of California, Berkeley, California 94720
and Physical Biosciences Division, Lawrence Berkeley National Laboratory, Berkeley, California 94720

(Received 2 May 2005; accepted 6 April 2006; published online 16 June 2006)

Using the nonperturbative approach to the calculation of nonlinear optical spectra developed in a foregoing paper [Mančal *et al.*, J. Chem. Phys. **124**, 234504 (2006), preceding paper], calculations of two-dimensional electronic spectra of an excitonically coupled dimer model system are presented. The dissipative exciton transfer dynamics is treated within the Redfield theory and energetic disorder within the molecular ensemble is taken into account. The manner in which the two-dimensional spectra reveal electronic couplings in the aggregate system and the evolution of the spectra in time is studied in detail. Changes in the intensity and shape of the peaks in the two-dimensional relaxation spectra are related to the coherent and dissipative dynamics of the system. It is shown that coherent electronic motion, an electronic analog of a vibrational wave packet, can manifest itself in two-dimensional optical spectra of molecular aggregate systems as a periodic modulation of both the diagonal and off-diagonal peaks. © *2006 American Institute of Physics*. [DOI: 10.1063/1.2200705]

I. INTRODUCTION

The requirement for optical spectroscopy to provide useful information on increasingly complex, multicomponent systems is fueled by advances over a wide range of areas from biology to materials science. In response, multidimensional techniques have been developed initially for nuclear motions (infrared and Raman)[1–14] and more recently for electronic interactions.[15–23] Theory and computational methods have been quite extensively developed for the infrared and Raman spectroscopies[2,4,8,24–26] and even for optical spectroscopies of multilevel electronic systems.[27,28] However, the level structure and dynamical mechanisms relevant to multichromophore electronic spectroscopy are quite distinct from their vibrational relatives or relaxation free electronic state manifold, and new methods must be developed for prediction and analysis of spectral features.

Recently, Brixner *et al.*[23] and Cho *et al.*[29] have described experiments and theoretical analysis of two-dimensional (2D) photon echo spectra of the seven-bacteriochlorophyll containing Fenna-Matthews-Olson (FMO) complex.[30,31] In related work, the connection between the two-color photon echo peak shift[32,33] and the 2D photon echo spectra was explored.[34] The theoretical approach in both cases was based on the perturbative approach which, largely as a result of Mukamel's classic text,[35] enabled rapid and efficient calculation of the dynamics and 2D spectral evaluation. Because of the approximation made in Ref. 29, the very short-time dynamics could not be calculated. In this paper we take a different approach to the calculation of 2D spectra based on the nonperturbative approach described in the companion paper[36] (Paper I). The main advantage of the nonperturbative (NP) method is that it allows description of system dynamics in a very flexible way including a rather general description of relaxation and dephasing processes and a numerically exact treatment of the system-field interaction. In the present paper we apply the NP approach to calculate 2D optical photon echo spectra of an excitonically coupled molecular dimer. We study the 2D spectrum of the dimer as the simplest molecular aggregate, in order to clarify the relation between the content of 2D spectrum and the system dynamics when both coherent and dissipative features are present. Since we are interested in coherent effects, the Förster theory cannot be used to describe ultrafast photoinduced exciton dynamics which is a nonequilibrium process. In this case one needs a more detailed dynamical description such as the Redfield theory. We model the dissipative exciton dynamics using the Frenkel-exciton model and Redfield theory.

Although coherent nuclear motion (vibrational wave packets) is a standard feature of ultrafast optical spectroscopy,[37–47] the observation of electronic coherence in molecular systems does not appear to have been definitively reported. A number of theoretical studies have suggested that electronic coherence might also be observable in, for example, ultrafast electron transfer (ET) reactions.[48–54] In the short-time dynamics of such systems, large amplitude quantum beats are potentially observable, but to the best of our knowledge they have not been reported in spectroscopic signals. This is perhaps not surprising as there are a number of natural obstacles to such an observation: (i) in the so-called internal case where the ET occurs between the same electronically coupled states as the optical transition, the electronic coherence (EC) period is very short (a few femtoseconds) and the effect cannot be resolved with currently

[a)]Electronic mail: grfleming@lbl.gov

available techniques and (ii) in the case of a three-state ET system with an optical transition between a ground state and an excited state which in turn consists of two coupled electronic states, one usually has a rather long EC period (typically few hundred femtoseconds); however, the very fast dephasing time present in real systems (typically 10–100 fs) destroys the coherent superposition and precludes its observation. The situation in an excitonic manifold of a coupled multichromophore aggregate may be more favorable for the observation of electronic coherence. First, the oscillation periods corresponding to the energy gaps between pairs of exciton states can often be in an intermediate time regime: short enough to survive dephasing and long enough to be resolved with femtosecond 2D spectroscopy. Second, in photosynthetic light harvesting complexes, the reorganization energy is remarkably small[55] which makes such systems attractive candidates for the observation of electronic coherence. By means of nonperturbative calculations on a model dimer system, we explore how electronic coherence is manifested in 2D photon echo spectroscopy with the aim of guiding experimental studies.

The paper is organized as follows. In Sec. II we briefly review the main ideas of NP approach and give definitions of the spectroscopic signals. The Hamiltonian of the dimer model system and the equations of motion including the Redfield theory for the description of the dissipation are introduced in Secs. III and IV, respectively. Section V presents the results of our calculations of 2D spectra of the dimer for different values of the system parameters and the discussion of the 2D spectral features that reflect the dimer dynamics with an emphasis on electronic coherence effects. Some estimations of the possible appearance of coherent effects in the 2D spectra of large aggregates are offered in that section, too. All details of the description of relaxation and dephasing in the dimer system within the Redfield theory are summarized in Appendices.

II. NONPERTURBATIVE CALCULATION OF NONLINEAR SIGNALS AND DEFINITION OF 2D OPTICAL SPECTRUM

In the foregoing paper[36] (Paper I) we presented a general nonperturbative approach to the calculation of nonlinear spectroscopic signals. The main idea of the method is to treat the system-field interaction (numerically) exactly by its explicit inclusion into the Hamiltonian

$$H_{\mathrm{tot}}(t) = H_{\mathrm{mol}} - \hat{\boldsymbol{\mu}} \cdot \boldsymbol{\mathcal{E}}(t), \tag{1}$$

in contrast to standard perturbative treatments.[35] We start with a short overview of the NP method; the details can be found in Paper I.

The main problem in NP approach is to extract the direction-resolved components from the total polarization obtained as the expectation value of the dipole operator:

$$\mathbf{P}(t) \equiv \mathrm{Tr}\{\hat{\boldsymbol{\mu}}\rho(t)\}. \tag{2}$$

In Paper I (Ref. 36) we extended the method developed by Seidner *et al.*[56] to the most general case of four-wave-mixing (FWM) experiments. We assume that the external electric field consists of three laser pulses: $\boldsymbol{\mathcal{E}}(t)=\Sigma_{n=1}^{3}\mathbf{E}_n(t)$, each pulse $\mathbf{E}_n(t)=\mathbf{e}_n E_n(t)\exp\{-i(\omega_n t)\}+\mathrm{c.c.}$ is characterized by its frequency ω_n, phase, $\phi_n \equiv \mathbf{k}_n\mathbf{r}$, polarization direction $\mathbf{e}_n$, and envelope $E_n(t)$. The overall nonlinear polarization consists of a number of contributions with different directions of propagation in space as a result of the interaction of the system with the fields having different wave vectors. The central result on which the NP approach is based is that in a general FWM experiment, a nonlinear signal of $(2N+1)$th order can only travel into directions given by a wave vector

$$\mathbf{k}_s - n_1(\mathbf{k}_1 - \mathbf{k}_3) + n_2(\mathbf{k}_2 - \mathbf{k}_3), \tag{3}$$

where $n_1+n_2=-(N+1),\ldots,N$. Consequently the signal depends only on the phase difference between the first and the third (δ_1) and the second and third (δ_2) pulses in the FWM sequence. By calculating the nonlinear signal with varying phase relations among the pulses, we can separate the spatial components of the nonlinear signal.

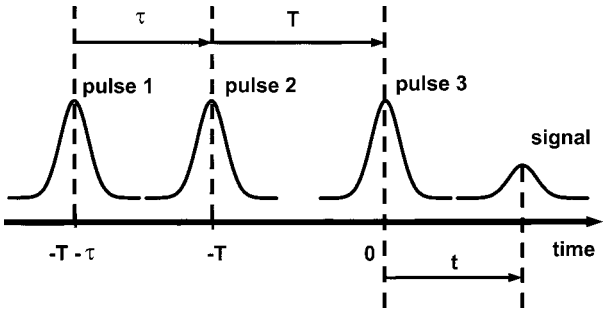

FIG. 1. The pulse scheme of a photon echo experiment. Three pulses with successive delays τ and T are applied to the system. The time origin is conventionally set to the middle of the third pulse. The photon echo signal arises at times $t>0$. In 2D spectroscopy we vary the first delay τ to record a two-dimensional signal (in τ and t) for a given delay T.

In Paper I we illustrated the method by its implementation for the calculation of 2D three-pulse photon echo spectra. The photon echo signal E_{k_s} is proportional to the component of the nonlinear polarization in the direction $\mathbf{k}_s=-\mathbf{k}_1+\mathbf{k}_2+\mathbf{k}_3$ (see Fig. 1) and can be detected using a heterodyne detection scheme.[22] Two-dimensional spectra are recorded for a given value of the delay T between the second and the third pulses (the population time, see Fig. 1) by successive frequency-resolved measurements of the photon echo signal for different values of the delay τ between the first and the second pulses (the coherence time). A conventional 2D spectrum is obtained by switching to the frequency domain via numerical Fourier transform:

$$S_{2\mathrm{D}}(\omega_\tau, T, \omega_t) \sim \int_{-\infty}^{\infty} dt \exp(-i\omega_t t) \times \int_{-\infty}^{\infty} d\tau \exp(i\omega_\tau \tau) E_{k_s}(\tau, T, t). \tag{4}$$

III. DIMER MODEL SYSTEM

A dimer is the simplest prototype of a molecular aggregate. To describe correctly the third-order nonlinear spectroscopic experiment on molecular aggregates, one has to ac-

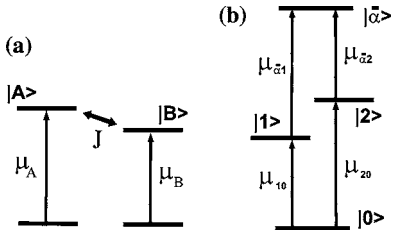

FIG. 2. The electronic-level scheme of the model dimer system. (a) Heterodimer in the molecular electronic states representation, with transition moments μ_A and μ_B and the excitonic coupling J. (b) Heterodimer complex after diagonalization, i.e., in the eigenstate (exciton) representation.

count for one- and two-exciton states. We consider two molecules A and B with intermolecular coupling J (see Fig. 2), and the system Hamiltonian formulated in terms of molecular electronic states is written using the standard Frenkel-exciton model as

$$H_{\text{dimer}} = (H_A^g(Q) + H_B^g(Q))|0\rangle\langle 0| + H_A^e(Q)|A\rangle\langle A| + H_B^e(Q)|B\rangle\langle B| + J(|A\rangle\langle B| + |B\rangle\langle A|) + (H_A^e(Q) + H_B^e(Q))|AB\rangle\langle AB|. \quad (5)$$

Here $|0\rangle$ denotes the collective state of the dimer with both molecules in the ground state, $|A\rangle$ ($|B\rangle$) denotes the electronic state when the molecule $A(B)$ is excited, and $H_i^g(Q)$ and $H_i^e(Q)$ are the nuclear Hamiltonians of ith molecule ($i=A,B$) in the ground and excited states, respectively. Further, $|AB\rangle$ denotes the electronic state when two molecules are excited simultaneously (doubly excited state), and coupling J describes the Coulombic interaction between excitations located on sites A and B. The nuclear Hamiltonians read

$$H_A^g(Q) = \epsilon_A^g + T_A + V_A^g(Q), \quad (6)$$

$$H_A^e(Q) = \epsilon_A^e + T_A + V_A^e(Q), \quad (7)$$

and similarly for B, where $\epsilon_A^g(=0)$ and ϵ_A^e are the electronic energies of molecule A in the ground and excited (i.e., excitation energy) states, respectively. The quantities $V_A^g(Q)$ and $V_A^e(Q)$ are the ground- and excited-state nuclear potential energy surfaces, respectively, and T_A is the kinetic energy of the nuclei. The molecular electronic states form a complete basis set: $|0\rangle\langle 0| + \Sigma_{i=A,B}|i\rangle\langle i| + |AB\rangle\langle AB| = 1$.

For the description of the system-field and system-bath interactions, we switch to the eigenstate representation, the so-called exciton basis. After diagonalization of the Hamiltonian with respect to the electronic energies, we obtain a set of eigenstates: two single-exciton states $|\alpha\rangle$ and one two-exciton state $|\bar{\alpha}\rangle$ with energies ϵ_α and $\epsilon_{\bar{\alpha}}$, respectively. The exciton states are constructed from the molecular states as

$$|\alpha\rangle = \sum_i C_i^{(\alpha)}|i\rangle = C_A^{(\alpha)}|A\rangle + C_B^{(\alpha)}|B\rangle, \quad \alpha = 1,2, \quad (8)$$

$$|\bar{\alpha}\rangle = \sum_{i>j} C_{ij}^{(\bar{\alpha})}|ij\rangle = |AB\rangle. \quad (9)$$

The diagonalization of the dimer Hamiltonian can be easily performed analytically. The elements of the transformation matrix are

$$C_A^{(2)} = \cos\theta, \quad C_B^{(2)} = \sin\theta,$$

$$C_A^{(1)} = -\sin\theta, \quad C_B^{(1)} = \cos\theta, \quad (10)$$

with

$$\tan 2\theta = \frac{2J}{\epsilon_A - \epsilon_B}, \quad (11)$$

and the eigenenergies read

$$\epsilon_{2,1} = \tfrac{1}{2}(\epsilon_A + \epsilon_B) \pm \tfrac{1}{2}\sqrt{(\epsilon_A - \epsilon_B)^2 + 4J^2}, \quad (12)$$

$$\epsilon_{\bar{\alpha}} = \epsilon_A + \epsilon_B. \quad (13)$$

In the exciton basis the dipole operator takes the form

$$\mu = \sum_\alpha \mu_{\alpha 0}|\alpha\rangle\langle 0| + \mu_{\bar{\alpha}\alpha}|\bar{\alpha}\rangle\langle\alpha| + \text{c.c.}, \quad (14)$$

with the matrix elements between the ground and one-exciton states given by

$$\mu_{20} = \cos\theta\mu_A + \sin\theta\mu_B,$$

$$\mu_{10} = -\sin\theta\mu_A + \cos\theta\mu_B, \quad (15)$$

where μ_i describes an optical transition in the ith molecule. For transitions between the one- and two-exciton states, we obtain

$$\mu_{\bar{\alpha}2} = \cos\theta\mu_B + \sin\theta\mu_A,$$

$$\mu_{\bar{\alpha}1} = -\sin\theta\mu_B + \cos\theta\mu_A. \quad (16)$$

An analogous transformation to that of the electronic energies from the diagonalization also operates on the nuclear potentials $V_A^g(Q)$, etc. Since we diagonalized only with respect to the electronic energies, certain off-diagonal terms remain nonzero. These terms lead to the transitions between the eigenstates and they will be treated within the Redfield theory[57] as described in the next section.

IV. EQUATIONS OF MOTION

As we stressed before, the NP approach has the advantage of including the system-field interaction explicitly into the equations of motion and thus avoiding the cumbersome numerical evaluation of multitime response functions. The conventional approach to account for dissipative effects in complex systems is the reduced density matrix (RDM) formalism leading to the Redfield equations. In this section, we outline the RDM approach and present its application to the dimer system.

A. Reduced density matrix description

In photosynthetic systems, excitation energy is transported between pigments of the antenna to allow the energy to reach the reaction centers. The optical excitation process is much faster than the response of the nuclear degrees of freedom resulting in a creation of a nonequilibrium nuclear wave packet in the excited electronic state. The motion of vibrational wave packets has been observed as coherent oscillations in pump-probe signals during energy transfer in the

photosynthetic reaction center and antenna complexes of bacteria.[37–40,58] Naturally, with short femtosecond pulses, it is also possible to create a coherent (electronic) excitonic superposition of states. In this paper we discuss the possibility of such an effect—electronic or excitonic coherence—in the ultrafast energy transfer in molecular aggregates.

During the equilibration process part of the excitation energy is dissipated into the surroundings. To describe dissipation in the system, it is a conventional practice to adopt a system-bath approach that assumes a separation of the problem into a relevant (system) part and an irrelevant (bath) part that is regarded as a dissipative environment. The approach leads to a RDM description (see Ref. 57 for details). This theory has been successfully applied to many problems, the most intensively studied being the photoinduced ultrafast electron[48,52,59] and energy transfer[60–63] problems. For the Hamiltonian (5) it is possible to separate system (electronic), bath (nuclear), and the interaction parts and write formally

$$H_{\mathrm{mol}} = H_{\mathrm{S}} + H_{\mathrm{B}} + H_{\mathrm{SB}}. \tag{17}$$

Since we concentrate here only on excitonic wave packets, the separation is natural: The system consists only of the electronic part of the molecular Hamiltonian, while it is assumed that the nuclear (vibrational/phonon) modes are only weakly coupled to the system and can be described as a heat bath. If one wants to study the (coherent) vibrational effects in exciton dynamics, then the system has to be redefined to include one (or several) vibrational modes explicitly[64,65] as it is done in the electron transfer problem.[48,52,59]

In the system-bath approach, in order to derive the equation of motion for the system, we can switch from the entire (system plus bath) phase space to that of the system only. Neglecting the effect of the field-matter coupling on dissipation and employing perturbation theory with respect to the system-bath interaction, the bath variables can be averaged out in the standard way.[57] Thus, one arrives at an equation for the reduced density matrix ρ, which is defined as the trace over all bath variables of the full density matrix, W: $\rho = \mathrm{Tr}_B\{W\}$, and depends only on system degrees of freedom. The RDM $\rho(t)$ is the primary quantity describing the relevant *system* dynamics. A dissipative equation of motion for the RDM, in a general form, reads

$$\partial_t \rho(t) = -iL\rho(t) + \mathcal{D}(t;\rho(t)), \tag{18}$$

where L is an effective system Liouvillian and the operator $\mathcal{D}(t;\rho(t))$ describes the relaxation dynamics induced by the system-bath interaction. Furthermore, introducing the Markovian approximation for the relaxation operators (see Refs. 57 and 66 for details), we obtain the well-known Redfield equation for the reduced density matrix which is written explicitly as follows:

$$\partial_t \rho(t) = -i[(H_{\mathrm{S}} - \boldsymbol{\mu}\mathbf{E}(t)), \rho(t)] + R\rho(t), \tag{19}$$

where R is the relaxation or Redfield operator which is specified in detail in Appendix A. The Redfield operator contains the relaxation and dephasing rates that are calculated directly from the interaction Hamiltonian H_{SB}. We further employ the so-called secular approximation and the Redfield tensor reduces to two rate matrices—one for relaxation and the other for dephasing rates (see Appendix B). The presence of the system-field interaction term in the Liouvillian [commutator part of Eq. (19)] underlines the fact that we work within the NP approach.

B. Rotating wave approximation

With the general equation of motion for the RDM (19) in hand, we can calculate the dynamics of the system under the influence of any type of laser field. From the general form we can derive equations of motion for the RDM elements $\rho_{0\alpha}$ and $\rho_{\alpha\bar{\alpha}}$ which are relevant to the calculation of the polarization [see Eq. (24)]. We introduce the rotating wave approximation (RWA) into the equations of motion to avoid rapidly oscillating terms in Eq. (19) that would present a problem in the numerical solution of the equations and to obtain the total polarization from which the spatial components of the signal can be extracted. As discussed in Ref. 36, the method for extraction of the polarization components requires the RWA. We assume in addition that all laser pulses have the same carrier frequency: $\omega_n = \Omega$ for $n = 1,2,3$. (The generalization for the case of different frequencies is rather straightforward.) Thus, the electric field can be written as

$$\mathcal{E}(t) = \mathbf{E}(t)e^{-i\Omega t} + \mathbf{E}^*(t)e^{i\Omega t}, \tag{20}$$

where

$$\mathbf{E}(t) = \sum_{n=1}^{3} \mathbf{e}E_n(t)e^{-i\phi_n}. \tag{21}$$

The RWA means neglecting all the terms in the equation of motion that oscillate faster than $e^{\pm i\Omega t}$. Therefore we use the following ansartz for the off-diagonal elements of the RDM:

$$\rho_{\alpha 0} = \sigma_{\alpha 0}e^{-i\Omega t}, \quad \rho_{\bar{\alpha}\alpha} = \sigma_{\bar{\alpha}\alpha}e^{-i\Omega t}, \quad \rho_{\bar{\alpha}0} = \sigma_{\bar{\alpha}0}e^{-i2\Omega t}. \tag{22}$$

We then obtain the equations of motion where only the slowly varying functions [pulse envelope function $\mathbf{E}(t)$ and RDM elements σ_{ij} and ρ_{ii}] are present. The particular equations of motion for our dimer problem can be found in Appendix D.

The closed set of Eqs. (D1)–(D6) is solved by standard methods with the initial condition (before the first interaction with a field)

$$\rho(0) = |0\rangle\langle 0|. \tag{23}$$

The relaxation and dephasing rates entering these equations are given in Appendix C. A similar type of analysis can be performed for any type of molecular system.

C. Calculation scheme

The key quantity for the calculation of the nonlinear optical signals of the system is the polarization. For the specific form of the dipole operator (14), the polarization (2) becomes

$$\mathbf{P}(t) = \sum_{\alpha} \mu_{\alpha 0}\rho_{0\alpha}(t) + \sum_{\alpha,\bar{\alpha}} \mu_{\bar{\alpha}\alpha}\rho_{\alpha\bar{\alpha}}(t). \tag{24}$$

In Paper I we described how to calculate 2D spectra using the NP method. The application of the method to molecular

aggregates can be summarized in the following recipe: (1) define the molecular Hamiltonian (site energies and couplings), (2) diagonalize the Hamiltonian and obtain the exciton states, (3) calculate the Redfield tensor (relaxation and dephasing rates), (4) solve the Redfield equation (19) with a selected set of laser pulse phases δ_1 and δ_2 and get RDM $\rho(t)$, (5) calculate $\mathbf{P}(t;\delta_1,\delta_2)$ [Eq. (24)], (6) repeat steps 1–5 for different values of δ_1 and δ_2 and extract the component P_{k_s} according to the method described in Sec. II, and (7) calculate the desired spectroscopic signal, for example, the 2D photon echo spectrum [Eq. (4)]. Static inhomogeneity is taken into account by averaging the results over an ensemble of different realizations of the Hamiltonian. As we discussed in Paper I, the presence of inhomogeneity in the system is vital for the delayed time domain photon echo effect to appear.[35] The inhomogeneous width describes the distribution of transition energies of the monomers in the ensemble. We might expect the distributions of the two monomers forming the dimer to be correlated to some degree. In the present work we will only study limiting cases of noncorrelated and fully correlated/anticorrelated monomers.

V. 2D SPECTRA OF A DIMER MODEL SYSTEM: NUMERICAL RESULTS AND DISCUSSION

In this section we utilize the NP calculation scheme given above for the numerical calculations of 2D photon echo spectra of a model dimer system. We discuss various spectral features in the 2D spectrum calculated by the NP method. Some of these features, such as the appearance of cross peaks in the 2D spectrum due to the excitonic coupling and the shapes of the peaks, are the generic properties of the two-dimensional spectra (both optical and IR) which have been discussed in detail in many experimental and theoretical (within a perturbative approach) works (see review papers.[3,8,25,26,29,67] We also show several features in the calculated 2D relaxation spectrum that appear to be novel and had not been reported before; they originate from the complex interplay of coherent and dissipative excitonic dynamics.

As in Ref. 36, we use a simple fourth-order Runge-Kutta (RK) method[68] with fixed time step to solve the equations of motion. The total complex polarization is outputted with a step of 2 fs over the time delays τ and t in the interval from 0 to 600 fs. The time step of the RK method is chosen as an integer fraction of the output time and tested for cumulative error by comparing calculations with a different time step. The photon echo signal is then extracted using the discrete Fourier transform method described in Ref. 36. The 2D trace is calculated by a standard fast Fourier transform algorithm with suitable zero padding for times higher then 600 fs. As in Ref. 36, the intensity of the electric field is chosen so that the population of the excited state is less than 1% to ensure that contributions from higher nonlinearities remain negligible.

A. Dimer versus two uncoupled two-level systems

We start with a simple example which illustrates one of the main advantages of 2D optical spectroscopy. In Fig. 3 we compare the 2D spectra of two uncoupled monomers ($J=0$) and of the dimer (excitonically coupled monomers, $J=300$ cm^{-1}) calculated at $T=0$. The parameters have been chosen to produce the same energy separation between the two diagonal peaks in both spectra and, since the diagonal slice reflects the linear absorption spectrum, this leads to similar linear absorption spectra, each showing a doublet structure. In the calculation we used the following system parameters: $\epsilon_A=16\,360$ cm^{-1}, $\epsilon_B=15\,640$ cm^{-1}, and $d_A=d_B=1$ ($\boldsymbol{\mu}_A=d_A\mathbf{n}$ and $\boldsymbol{\mu}_B=d_B\mathbf{n}$, where $\mathbf{n}$ is a unity vector in the direction of the dipole moment) in case of two monomers and $\epsilon_A=16\,200$ cm^{-1}, $\epsilon_B=15\,800$ cm^{-1}, $J=300$ cm^{-1}, $d_A=1$, and $d_B=-0.23$ for the dimer. The other parameters are the inhomogeneous distribution width of the monomer transitions, $\Delta=200$ cm^{-1}, the pulse-carrier frequency $\Omega=16\,000$ cm^{-1} (excitation in the center of one-exciton manifold), and the pulse duration $\tau_{\text{pulse}}=5$ fs. As this laser pulse is very short the validity of the RWA needs to be discussed. At $\Omega=16\,000$ cm^{-1} the laser pulse completes about 2.5 optical cycles during its full width at half maximum (FWHM) and the RWA neglects contributions that oscillate with frequency about 2Ω, i.e., those that complete about five optical cycles, against those arising from the relatively slowly varying envelope. In Ref. 69, Ferro *et al.* showed by reformulating the RWA in the frequency domain that the RWA neglects the frequency overlap between the negative frequency field and the positive frequency susceptibility. If the laser pulse spectrum is well confined to its expected side of zero, it is not responsible for the breakdown of the approximation. The frequency FWHM of a 5 fs laser pulse is about 6000 cm^{-1} which is significantly less then the energy gap of 16 000 cm^{-1} and the RWA can be assumed to be still valid for these parameters.

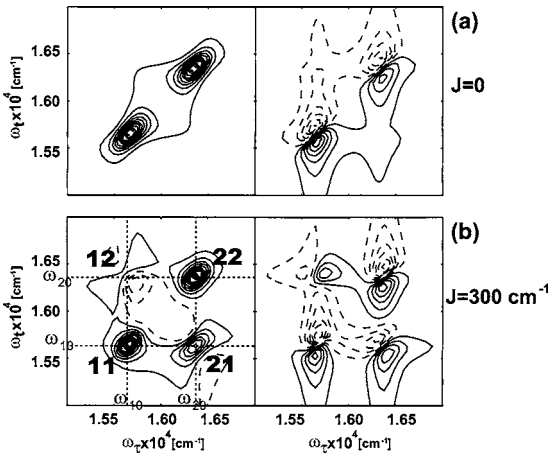

FIG. 3. Comparison of the 2D spectra (a) of two uncoupled monomers ($J=0$) and (b) of the dimer ($J=300$ cm^{-1}). The parameters have been chosen to produce the same energy separation between two diagonal peaks. The electronic coupling between two monomers is revealed by the appearance of the cross peaks 21 and 12 in the 2D spectrum. Contour lines are drawn in 10% intervals at $-95\%,\ldots,-5\%,5\%,\ldots,95\%$ for the absorptive real parts (left column) and refractive imaginary parts (right column) of $S_{2D}(\omega_\tau,T,\omega_t)$. The level of 100% is determined from the highest peak value within the spectrum. Solid contour lines correspond to positive and dashed lines to negative amplitudes.

Let us first consider the uncoupled system [Fig. 3(a)]: It is simply two two-level systems having different excited-

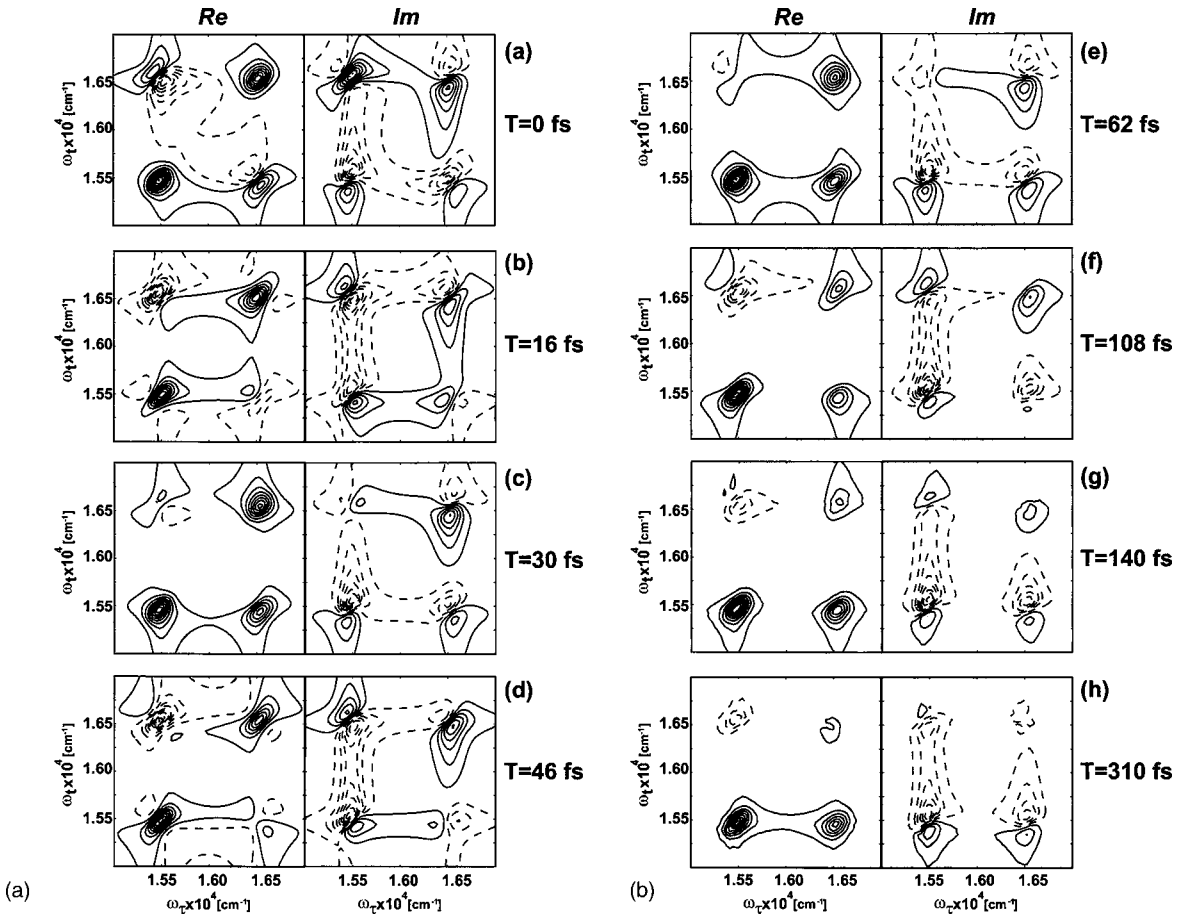

FIG. 4. 2D relaxation spectra of the dimer calculated at population times (a) $T=0$ fs, (b) $T=16$ fs, (c) $T=30$ fs, (d) $T=46$ fs, (e) $T=62$ fs, (f) $T=108$ fs, (g) $T=140$ fs, and (h) $T=310$ fs. The exciton energy splitting corresponds to the modulation period of 31 fs. Population times in (a), (c), and (e) and (b), (d), (f), and (g) correspond to the maxima and minima of periodic modulations (electronic coherence effect), respectively. At longer population times, $T=310$ fs (h), the intensity is transferred from the diagonal peak 22 to the cross peak 21 due to the population relaxation. The shape of the peaks also varies with the population time (see the discussion in the text).

state energies. The 2D spectrum of the two-level system was discussed in detail in a previous paper.[36] The 2D spectrum contains only two diagonal peaks appearing along the diagonal axis, $\omega_\tau=\omega_t$, which can be obtained as a combination of two spectra of two-level system shifted along the diagonal by the value $\Delta\epsilon_{21}$. The figure shows that, for example, excitation at ω_{20} causes emission only at ω_{20} but not at ω_{10}. Some features which one may erroneously attribute to the cross peaks appear because of the overlap of the two spectra.

In the 2D spectrum of the dimer [$J=300$ cm^{-1}, Fig. 3(b)] additional—cross (or off diagonal)—peaks appear due to the coupling between the monomers. The 2D spectra are very informative; they show how excitation at one frequency affects the spectrum (e.g., increased emission or absorption) at other frequencies (see, e.g., recent reviews[25,26]). In the dimer, for example, excitation at ω_{20} may cause emission not only at the same frequency but, because of the coupling, also at ω_{10}. This leads to the appearance of cross peak at the position we denote by 21. In the present paper we use the peak notation where the first number indicates the position of the peak on the excitation frequency axis ω_τ and the second on the emission frequency axis ω_τ [see Fig. 3(b)]. In general, for aggregates consisting of many molecules, the positions of the cross peaks, if they appear in the spectrum, show immediately the presence of couplings between the corresponding chromophores. A full interpretation of a 2D spectrum can give quantitative information about the system parameters: The intensity of the cross peaks depends on the electronic coupling strength J and on dipole moments (absolute values and mutual orientations) of the transitions contributing to this peak. One cannot obtain such type of information from, e.g., pump-probe spectra.

B. Dimer relaxation spectra

Next, we focus on the evolution of the dimer 2D spectra with increasing population time T. In Fig. 4 we present a series of 2D spectra calculated for a series of population times: $T=0$, 16, 30, 46, 62, 108, 140, and 310 fs; we will refer to these as 2D relaxation spectra.[8,16] The dynamics of the density matrix is obtained from the Redfield equation as described in Sec. V. The system parameters are $\epsilon_A=16\,200$ cm^{-1}, $\epsilon_B=15\,800$ cm^{-1}, $J=500$ cm^{-1}, $d_A=1$, and $d_B=-0.15$. Other parameters are the same as in the previous example [Fig. 3(b)]. The chosen system parameters produce an initial 2D spectrum [$T=0$ fs, Fig. 4(a)] with two diagonal peaks of roughly equal intensities and two well-resolved cross peaks. After the system has an opportunity to evolve

during the population period [$T>0$, Figs. 4(b)–4(h)], a number of features can be observed in the 2D relaxation spectra: appearance and disappearance of cross peaks, modulations of the diagonal peak intensities, intensity redistribution between the peaks, and changes of the peak shapes as T increases. Looking at the spectra in more detail, we notice that there are two processes with different dependences on T: a periodic behavior (appearance and disappearance of cross peaks and smaller intensity modulations of diagonal peaks) at short times and a monotonous transfer of the intensity from the diagonal peak 22 to the cross peak 21 at longer population times.

1. Coherent electronic motion

Let us first consider the short-time periodic behavior of the peaks. Figure 4(b) shows that a very strong negative cross peak, 12, quickly grows and reaches its maximum at $T=16$ fs and on the same time scale the second cross peak, 21, loses its intensity and becomes negative. Correspondingly, the absolute value spectrum (not shown here) would show the appearance of a new peak 21 and the disappearance of a peak 12. When T exceeds 16 fs, the process is reversed: The negative peak 12 quickly loses its intensity and peak 21 grows back [see Fig. 4(a) which corresponds to $T=30$ fs]. The observed features cannot be attributed to the pulse overlap effect: Calculations performed for different pulse durations, $\tau_{\text{pulse}}=30$ fs and $\tau_{\text{pulse}}=2$ fs, show the same behavior (maximum of the negative peak 12 at a population time T of 16 fs) irrespective of the pulse duration.

Figures 4(d)–4(g) which correspond to values of T beyond the pulse overlap region, also show strikingly periodic behavior. Clearly, the effect is entirely due to the system dynamics. The periodic behavior of peaks ("quantum beats") in the dimer 2D spectrum is the manifestation of coherent electronic motion. Similar quantum beats associated with electronic coherence have been shown theoretically to be present in the population dynamics in the electron transfer problem.[52,54] In excitonically coupled molecular complexes, short excitation pulses prepare a coherent superposition of excitonic states. Oscillatory responses observed earlier in the photosynthetic complexes[37–40] are associated with the motion of *vibrational* wave packets. Here one could speak of *excitonic* wave packets or *electronic coherence* (determined by the off-diagonal elements of the density matrix). A complementary interpretation can be given in terms of the molecular states. Because of the presence of strong coupling between two monomers, the probability of find the system, for example, in the state $|A\rangle$ when initially it was in the state $|B\rangle$ is a periodic function with a period corresponding to the exciton energy splitting $\Delta\epsilon_{21}=\sqrt{(\epsilon_A-\epsilon_B)^2+4J^2}$. The observed modulation period of the peaks in the dimer 2D spectrum, $T_{\text{EC}}=31$ fs, exactly corresponds to the $\Delta\epsilon_{21}$ value. The periodic behavior is clearly seen from Figs. 4(b)–4(g) where the population times were chosen to correspond to minima and maxima of the oscillations. A similar modulation rule was determined recently by Khalil *et al.*[70] from experimentally measured 2D infrared (IR) spectra. In that case, obviously, the modulation of the peaks resulted from vibrational wave packet motion. System parameters which give a large exciton splitting (and consequently a short modulation period) have been chosen to emphasize the periodic behavior. Changing the exciton splitting (via $\Delta\epsilon_{AB}$ and/or J) changes the modulation period, as described above.

For an intuitive explanation of the appearance of quantum beats in 2D spectra, it is helpful to use "perturbative" language.[2,6,26,71] Let us first consider the appearance/disappearance of cross peaks. There are two types of contributions to the cross peaks: (i) those not dependent on T that involve Feynman diagrams when the system is in the exciton population state (ρ_{22}, ρ_{11}, and ρ_{00}) during the population period and (ii) oscillating contributions which involve the diagrams describing the system in an exciton-coherence state (ρ_{12} and ρ_{21}; note that these are coherences within the one-exciton manifold but not inter-band coherences). Constant contributions are better seen in the real part of the 2D spectrum at $T=(2k+1)T_{\text{EC}}/2$, $k=0,1,\ldots$, [Figs. 4(b), 4(d), and 4(f)] when the oscillating contributions disappear. The intensities of these constant contributions (strong negative peak 12 and weak positive peak 21) are determined by the system parameters, in particular, by combination of all dipole moments.[2,8,29] At $T=2kT_{\text{EC}}/2$ [Figs. 4(a), 4(c), and 4(e)] the oscillating contributions reach their maximum values and we see an amplitude decrease of the negative peak, 12, in parallel with a growth of the positive peak, 21. In the absolute value spectrum this effect would manifest itself as a periodic appearance/disappearance of cross peaks.

The EC also modulates the diagonal peaks, though this is not clearly seen in Fig. 4. The 2D spectra shown here are contour plots which have been scaled to the maximum value for each value of T. Therefore, as long as the intensity of the diagonal peak is the largest in the spectrum, the diagonal peaks appear unchanged even though they might undergo significant amplitude changes. Some indications of the dynamics in the diagonal peaks come from changes in their shape (see Sec. V B 3 below). To show that diagonal peaks are also sensitive to the motion of the excitonic wave packet, in Fig. 5 we have plotted a cut of the 2D spectrum along the diagonal using absolute amplitudes (without normalization). We see that the diagonal peaks exhibit oscillatory behavior with the same modulation period (but much smaller amplitude than the cross peaks). A detailed explanation of the periodic behavior of the diagonal peaks can be obtained in the same way it was outlined for cross peaks. Depending on the amplitudes and resolution of the cross peaks, it may be easier, in some systems, to observe coherent excitonic motion from diagonal peak amplitudes, rather than cross-peak modulation.

The spectrum at $T=0$ [Fig. 4(a)] does not follow exactly the modulation behavior of the later-time spectra (there is a strong cross peak 12) because of the pulse overlap effect as described in Paper I for a two-level system. At $T\approx 0$ all three pulses (of finite duration) overlap and pulse sequences such as 2-3-1 contribute to the signal. These contributions are important only in the overlap region and quickly disappear as T increases.

The influence of electronic coherence gradually disappears at longer population times [Figs. 4(f)–4(h)]. Firstly, the coherent superposition is destroyed on the dephasing time

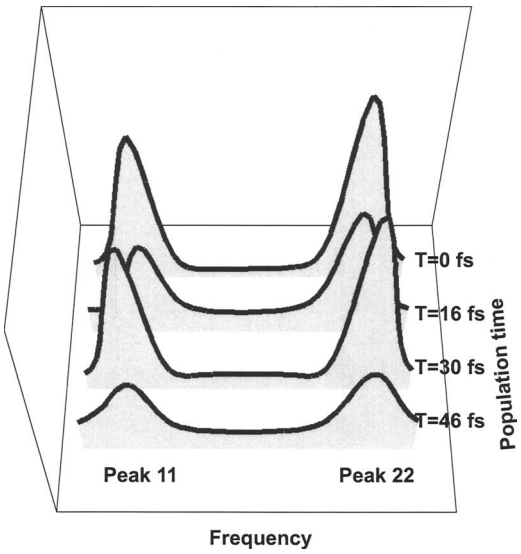

FIG. 5. The diagonal cuts of the real-part 2D relaxation spectra; absolute intensities (without scaling to the maximum value) are shown. Cuts correspond to the same population times (a) $T=0$ fs, (b) $T=16$ fs, (c) $T=30$ fs, (d) $T=46$ fs as in Fig. 4. The figure shows that diagonal peaks are also modulated by the motion of the excitonic wave packet.

$T_2=1/\Gamma_{12}$ due to destructive influence of the bath. Another process also becomes important, namely, population transfer which proceeds in the one-exciton manifold with a population relaxation time $T_1=1/\Gamma_{22}$. These two processes are related as demonstrated by the rate expression (C4). The dephasing and relaxation times in the system which we used in the calculation were defined to be 350 and 200 fs, correspondingly, to allow the observation of the motion of the excitonic wave packet for at least several periods.

At this point it is appropriate to note some important differences between 2D infrared and 2D optical spectra. Although the formal description of these two is very similar, there are significant differences between the vibrational and electronic spectroscopies. Most importantly, in the IR case one always has a ladder of states (e.g., for the simplest possible system, two coupled vibrations, there are two one-exciton states and three states in the two-exciton manifold—two overtones and one combination mode) and all possible transitions between these states have the oscillator strength of the same order of magnitude.[2,6,9,26,71,72] Consequently, many contributions nearly cancel each other; if anharmonicity is absent in the system, the cancellation is complete and the total signal is zero. This results in a nearly *symmetric* shape of 2D IR spectra. The situation is different in the case of 2D optical spectroscopy: The structure of the two-exciton manifold is qualitatively different, oscillator strengths of transitions could differ by order(s) of magnitude, and therefore there is no cancellation of various contributions. 2D optical spectra display some, often a considerable, degree of *asymmetry* about the diagonal as compared with typical 2D IR spectra.[23,29]

C. Population transfer

Population relaxation dynamics becomes dominant at longer population times. It induces intensity redistribution between the peaks as illustrated by Figs. 4(f)–4(h): The intensity of the diagonal peak 22 decreases while the intensity of the cross peak 21 peak increases with T. This "transfer" of the intensity reflects the exciton population relaxation: Since the downhill relaxation rate is larger than the uphill one (see Appendix C), the relaxation results in a larger population of the lower one-exciton state, $\rho_{11}(T)>\rho_{22}(T)$. Consequently, the probability of the emission from state $|2\rangle$, after initial excitation at ω_2, decreases while the same from state $|1\rangle$ increases. Within a perturbative approach this effect is described by the introduction of several additional Feynman diagrams involving a transfer process within the population period.[71,73,74]

In contrast to the coherent electronic motion, within our model, the population transfer is an incoherent process and proceeds irreversibly. Correspondingly, in the 2D spectra it appears as a monotonic transfer of the intensity. The effect of population relaxation becomes notable in 2D spectra at times $T>100$ fs. When the oscillations due to the EC effect are not yet damped completely, one can observe a "competition" between relaxation and electronic coherence. For example, the 2D spectra calculated at times $T=108$ and 140 fs [Figs. 4(f) and 4(g)], which correspond to the "minima" of the EC effect, $T=7T_{EC}/2$ and $T=9T_{EC}/2$, respectively, show a small-amplitude [compared to Fig. 4(b)] growth of the negative peak 12 along with a rather strong positive peak 21 and a weakened diagonal peak 22 (the manifestation of the population transfer). For population times larger than the relaxation time ($T>T_1$), the system reaches equilibrium in the one-exciton manifold. If the energy splitting between two eigenstates is large (compared to $k_B\mathcal{T}$), the system relaxes completely to the lower eigenstate, i.e., $\rho_{22}(T)=0$, and we can neglect the contribution to the signal from the higher one-exciton state. Then emission is possible only at ω_{10}: In Fig. 4(h) ($T=310$ fs) the spectrum is dominated by the two peaks 11 and 21. There is no correlation between excitation and emission frequencies. In this case, the 2D spectrum can be obtained as a product of the linear (one dimensional) absorption and emission spectra.[16] If, furthermore, the probabilities of excitation of both eigenstates were the same at $T=0$ fs, then we can expect equal intensities of the cross peak 21 and of the diagonal peak 11 as $T\to\infty$. As we mentioned, the 2D spectra are scaled to the maximum value for every time T; the absolute intensity of the peaks decays due to dephasing.

For this simple model system there are three main parameters obtained from the Redfield theory (see Appendices B and C): the population relaxation time $T_1=1/\Gamma_{22}$, the dephasing time $T_2=1/\Gamma_{12}$, and the homogeneous dephasing rate which is determined by the *intraband* coherence dephasing rate, e.g., Γ_{01}. We studied how these parameters influence the relaxation dynamics and manifest themselves in 2D spectra. Clearly a larger value for the population relaxation time T_1 simply shifts the peak intensity redistribution to a longer time scale. A longer dephasing time T_2 allows the electronic coherence effect (periodic behavior) to survive to longer population times, while a larger homogeneous dephasing rate broadens the peaks along both frequency axes, which results in larger overlap of the peaks.

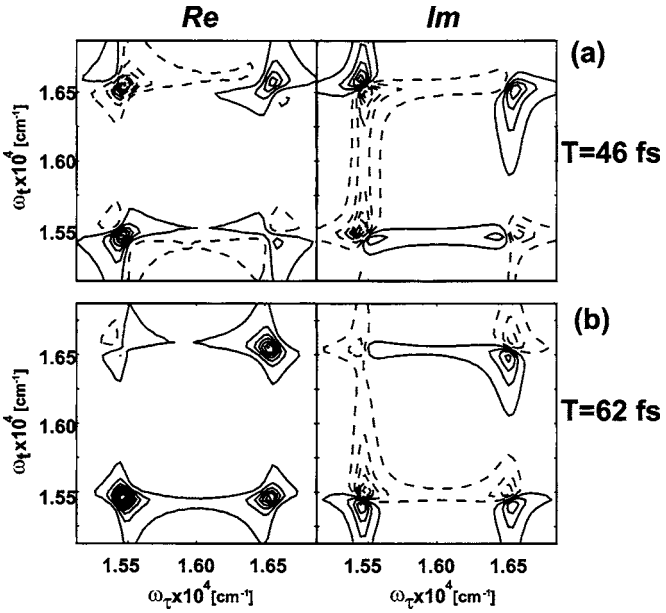

FIG. 6. Dimer homogeneously broadened ($\Delta=0$) 2D spectra which correspond to inhomogeneous ($\Delta=200\ \mathrm{cm}^{-1}$) case depicted on Figs. 4(d) and 4(e). Comparison shows that the form of 2D (inhomogeneous) spectrum can be obtained from elemental (homogeneous) spectral shapes. The presence of inhomogeneity can be understood in the way shown schematically on Fig. 7.

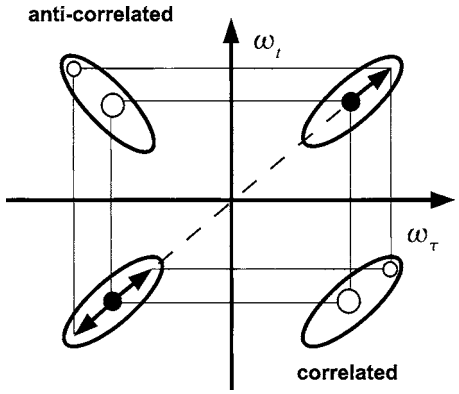

FIG. 7. The schematic explanation of the peak-shape formation for different correlation broadening cases. In the case where the energy fluctuations on both monomers are fully correlated (shown on the cross peak in the lower-right part of the figure), any change of the energy in one diagonal peak results in the same direction change in the other one. This shifts the position of the off-diagonal peak parallel with the diagonal. In the anticorrelated case (upper-left cross peak), the energetic changes in the diagonal peaks result in a shift of the cross peak that is orthogonal to the diagonal.

1. Shape of the peaks

The peaks change not only in intensity but also in their form. Remarkably, diagonal and cross peaks do this in a very different manner. Before population transfer becomes important [Figs. 4(b)–4(e)], the cross peaks are always diagonally elongated; only one of two peaks can be seen in the spectrum at a particular time and they appear/disappear with the opposite phase. As long as coherent electronic motion is present in the system, we also observe periodic behavior in the shape of the diagonal peaks. The effect is clearly seen from, e.g., Figs. 4(d) and 4(e) which represent the two opposite phases of the peak modulations (i.e., the two turning points of the electronic wave packet): When T corresponds to the minimum of the EC modulation, the diagonal peaks are strongly elongated along the diagonal [see both real and imaginary parts in Fig. 4(d), $T=46$ fs], and when T corresponds to the maximum of the EC modulation, the peaks are highly symmetric [Fig. 4(e), $T=62$ fs]. To explain the shapes of the spectral features of the inhomogeneously broadened spectra, one can utilize calculations without inhomogeneity in the way we did for the two-level system.[36] In Fig. 6 we present the calculated homogeneously broadened ($\Delta=0$) spectra for $T=46$ fs and $T=62$ fs corresponding to Figs. 4(d) and 4(e). Using these figures as elemental shapes for the dimer spectrum, we can predict the form of the spectral features for the inhomogeneously disordered system depending on the type of correlation between the fluctuations of the transition energies of the molecules forming the dimer.

At short times the shape changes of the diagonal peaks clearly arise from the electronic coherence. At longer times population transfer becomes important. The signature of this process can be seen first in Fig. 4(f): The negative cross peak, 12, starts to loose its diagonal orientation [compare with Fig. 4(d)] and the new (population-transfer-induced) cross peak 21 is entirely symmetric. At longer population times, this process evolves [Fig. 4(g)] and results in the "final" 2D spectrum form [Fig. 4(h)]. (This is valid as long as the inhomogeneity remains static.) The final shape of the diagonal peak can be understood in the same way as discussed for the two-level system (see the detailed discussion in Paper I): Due to the presence of inhomogeneous broadening in the system, peaks in the real part and the nodal line between the positive and negative regions in the imaginary part of the 2D spectrum are oriented along the diagonal, and the diagonal cut characterizes the inhomogeneous distribution.

Two-dimensional spectra contain information not only on line broadening mechanisms but also on correlation in the distribution of the transition energies of the coupled monomers. In particular, the form of the cross peaks is determined to a large extent by the correlation type.[4,8,75] This is illustrated schematically by Fig. 7 for the situation of two equal diagonal peaks. We consider three possible correlation types of fluctuations of the transition frequencies of two monomers, $\delta\omega_{10}$ and $\delta\omega_{20}$: (i) positively correlated, $\delta\omega_{10}=\delta\omega_{20}$, (ii) negatively correlated, $\delta\omega_{10}=-\delta\omega_{20}$, and (iii) independent (uncorrelated) fluctuations. (In the calculations throughout the paper we assumed the latter case.) When the energy fluctuations on both monomers are fully correlated, $\delta\omega_{10}=\delta\omega_{20}$, any change of the energy in one diagonal peak results in the same (direction and magnitude) change in the other peak. This shifts the position of the off-diagonal peak parallel to the diagonal and results in the diagonal-elongated shape of the cross peak as illustrated schematically by Fig. 7. In a similar manner one can understand the antidiagonal orientation of the cross peak in the case of negatively correlated fluctuations (the energetic changes in the diagonal peaks result in a shift of the cross peak that is orthogonal to the diagonal) and the symmetric shape of the cross peak in the uncorrelated case (the shift of the transition energy ω_{20} is combined with an arbitrary, i.e., same or the opposite sign, larger or smaller magnitude shift in ω_{10}).

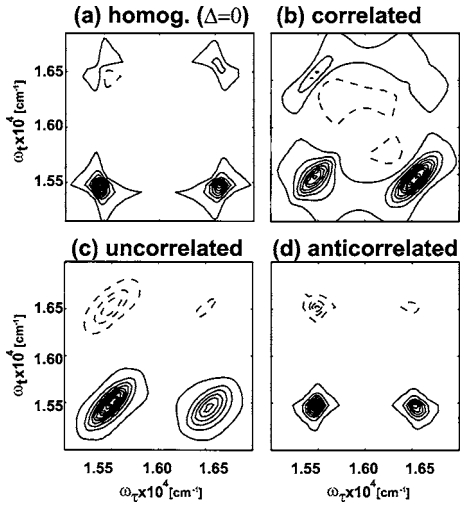

FIG. 8. The effect of correlated broadening on the dimer 2D spectra: real parts of the (a) homogeneous ($\Delta=0$) and inhomogeneous ($\Delta=400$ cm^{-1}) spectra calculated at time $T=310$ fs for the (b) fully correlated, (c) uncorrelated, and (d) fully anticorrelated fluctuations. Compare the shapes of the diagonal and cross peaks in different cases (see the discussion in the text).

In the calculation of 2D spectra, the described effect is combined with the actual elemental shapes (i.e., homogeneous spectra) to produce inhomogeneously broadened 2D spectra for a given type of correlation. As an example, homogeneous ($\Delta=0$) and inhomogeneous ($\Delta=400$ cm^{-1}) correlated, uncorrelated, and anticorrelated 2D spectra calculated at time $T=310$ fs are depicted on Fig. 8. The elemental shapes are slightly elongated peaks: diagonal peak oriented along the antidiagonal and cross peak along the diagonal [Fig. 8(a)]. The calculations confirm our qualitative analysis given above: Adding inhomogeneity to these elemental shapes, one gets remarkably different shapes of the peaks for the different correlation cases [Figs. 8(b)–8(d)]. In all three cases diagonal peaks become (to a different extent) diagonally elongated. In contrast, differently correlated transitions show different shapes of the cross peak:[8] Cross peak becomes elongated along the diagonal [Fig. 8(b)], keeps its shape but simply becomes broader symmetrically in all directions [Fig. 8(c)], and gets the antidiagonal orientation [Fig. 8(d)] in the cases of correlated, uncorrelated, and anticorrelated transitions, respectively. Thus, analysis of the form (ellipticity and orientation) of the peaks in experimentally measured 2D spectra should allow the degree of correlation between different transitions in the system to be qualified. It seems likely that such correlated fluctuations could significantly influence dynamical behavior in molecular complexes.

2. Summary and outlook

Our calculations reveal the influence of both coherent (excitonic wave packet motion) and incoherent (population transfer) effects in the photoinduced exciton dynamics of a model dimer system and their manifestation in 2D photon echo optical spectra. Similar phenomena should be found in larger complexes: periodic modulation (or even appearance/disappearance) of certain peaks after coherent excitation and intensity transfer from diagonal peaks to (possibly new) cross peaks as the result of population transfer. In multistate systems, new cross peaks may arise also due to coherence transfer between the pairs of eigenstates.[70,71] We will address these issues in a greater detail (including coherence transfer and a more general form of the Redfield equation) for larger systems in future work.

The first 2D optical spectrum of a molecular complex revealing resolvable and time-dependent cross-peak features has recently been reported by Brixner and co-workers[23,29] for the seven-bacteriochlorophyll-protein complex known as the FMO complex.[76] The analysis in Refs. 23 and 29 used a perturbative approach developed by Cho *et al.* and described in detail in Ref. 29. Within the limitations of the current Hamiltonian[29,76] the intermediate and long-time behavior of the FMO 2D spectra was quite well described. However, the very short-time behavior cannot be calculated with the approach of Cho *et al.*[29] because of the approximations used to obtain analytical approximations for the response functions. The nonperturbative approach described here can be used to investigate the short-time behavior of such a system.

The experimental data on the FMO complex show a very striking change in the amplitude of the lowest energy diagonal peak at $T=0$, 50, and 100 fs. This peak is very strong at $T=0$ fs, not detected at $T=50$ fs, and present with moderate intensity at $T=100$ fs.[23] Of course, these time intervals were selected for experimental convenience rather than with knowledge of the electronic coherence frequencies of the system, but such an oscillation of amplitude is strongly suggestive of the electronic coherence effects described here for the model dimer system. Numerical simulations and detailed analysis of the experimental data are underway, but in advance of this we can make estimates of the periods and upper limits of dephasing times expected in the FMO complex, based on the parameters used for the perturbative treatment.[29]

Table I shows the exciton splitting (difference) frequencies and their corresponding periods of pairs of eigenstates based on the Hamiltonian of Vulto *et al.*[76] The periods range from 60 to 980 fs. An upper limit to the dephasing time can

TABLE I. Difference frequencies $\omega_{(\alpha\beta)}$ (cm^{-1})/corresponding periods $T_{\alpha\beta}$ (fs) in the FMO complex.

Exciton energy E_n (cm^{-1})	1	2	3	4	5	6	7
1.121 12	0	150/222	243/138	302/111	336/100	499/67	537/64
2.122 62		0	92/365	152/220	186/180	349/96	387/88
3.123 55			0	59/564	93/360	256/130	294/113
4.124 14				0	34/980	197/168	235/141
5.124 48					0	163/204	201/164
6.126 11						0	38/877
7.126 49							0

be obtained from the relaxation rates between levels: $(\Gamma_{\alpha\beta})_{\min}=\frac{1}{2}(\gamma_{\alpha\beta}+\gamma_{\beta\alpha})$. This corresponds to an upper limit because pure dephasing ($\Gamma^{*}_{\alpha\beta}$) is neglected [see Eq. (C4)]. The experiments were performed at 77 K, making pure dephasing likely to be slower than at room temperature. Relaxation rates taken from a modified Forster/Redfield calculation[29] produce dephasing times in the range of 100–300 fs. Taking into account that the first minimum of the electronic coherence occurs at a half of the $T_{\alpha\beta}$ period, it seems very likely that the manifestation of electronic coherence will be observable even in a system with seven one-exciton states. Whether this phenomenon survives at physiological temperatures remains an open question, and detailed numerical calculations are clearly necessary to provide a definitive answer on the role of multiple states, temperature, coherence transfer, and the correlation of nuclear fluctuations on such a complex system. However, the level spacing (and thus the moderate oscillation frequencies) and the weak electron-phonon coupling common to all photosynthetic complexes[55,77] make photosynthetic pigment-protein complexes particularly favorable systems for the study of molecular electronic coherence.

VI. CONCLUSIONS

In this paper we have applied the nonperturbative method developed in Paper I (Ref. 36) to calculate 2D photon echo spectra of model dimer system and demonstrated the feasibility of including a sophisticated form of dissipative dynamics in the calculations. The different processes observed in the 2D spectra at different population times (periodic appearance/disappearance of cross peaks, intensity redistribution between the peaks, and changes of the peak shapes) were described in terms of two effects: coherent electronic motion and exciton population transfer. A qualitative understanding of the system dynamics is obtainable by a simple analysis of the time-dependent 2D spectra, and detailed numerical studies should enable extraction of quantitative information about the coherent and dissipative processes in multilevel molecular systems.

ACKNOWLEDGMENT

This work was supported by a grant from NSF.

APPENDIX A: REDFIELD EQUATIONS

In the eigenstate representation, the Redfield equation (19) takes the form

$$\partial_t\rho_{ij}(t)=-i\omega_{ij}\rho_{ij}(t)+\sum_{kl}R_{ijkl}\rho_{kl}(t)+i\mathbf{E}(t)\sum_{k}(\mu_{ik}\rho_{kj}-\rho_{ik}\mu_{kj}) \tag{A1}$$

with frequencies

$$\omega_{ij}=\epsilon_i-\epsilon_j,\quad i,j=0,\alpha,\bar{\alpha}. \tag{A2}$$

The first term on the right-hand side of Eq. (A1) describes the isolated system evolution, while the second and third represent its interaction with the dissipative environment (with the Redfield tensor responsible for system relaxation) and the external field, respectively.

The Redfield tensor elements $R_{\kappa\lambda\mu\nu}$ can be expressed as[48,52]

$$R_{\mu\nu\kappa\lambda}=\Gamma^{+}_{\lambda\nu\mu\kappa}+\Gamma^{-}_{\lambda\nu\mu\kappa}-\delta_{\nu\lambda}\sum_{\alpha}\Gamma^{+}_{\mu\alpha\alpha\kappa}-\delta_{\mu\kappa}\sum_{\alpha}\Gamma^{-}_{\lambda\alpha\alpha\nu}, \tag{A3}$$

where

$$\Gamma^{+}_{\lambda\nu\mu\kappa}=\int_0^\infty dt\langle\langle\lambda|H_{\mathrm{SB}}(t)|\nu\rangle\langle\mu|H_{\mathrm{SB}}|\kappa\rangle\rangle_{\mathrm{B}}e^{-i\omega_{\mu\kappa}t}, \tag{A4}$$

$$\Gamma^{-}_{\lambda\nu\mu\kappa}=\int_0^\infty dt\langle\langle\lambda|H_{\mathrm{SB}}|\nu\rangle\langle\mu|H_{\mathrm{SB}}(t)|\kappa\rangle\rangle_{\mathrm{B}}e^{-i\omega_{\lambda\nu}t}, \tag{A5}$$

$$H_{\mathrm{SB}}(t)=e^{iH_Bt}H_{\mathrm{SB}}e^{-iH_Bt}, \tag{A6}$$

and $\langle\cdots\rangle_{\mathrm{B}}$ denotes a thermal average over the bath.

For the dimer, the system-bath coupling is written in a general form as

$$H_{\mathrm{SB}}=\sum_{i=A,B}F_i|i\rangle\langle i|+(F_A+F_B)|AB\rangle\langle AB|, \tag{A7}$$

where the coupling function F_i describes the interaction of an excitation at site $|i\rangle$ with the bath. The damping matrices (A4) and (A5) are expressed in terms of the exciton overlap integrals (analogs of the Frank-Condon factors) and the Fourier transforms of the bath coupling functions (CFs). To calculate the elements of the Redfield tensor, we have to specify the form of the coupling function. We make the following simplifying assumptions about the nature of the system-bath (SB) interaction.

(i) The SB interactions at different sites are not correlated, i.e., each monomer is coupled only to localized vibrations. Thus, the two-site bath CF becomes $\langle F_i(t)F_j\rangle_{\mathrm{B}}=\delta_{ij}\,\langle F_i(t)F_i\rangle_{\mathrm{B}}$.

(ii) The SB interaction is treated within a linear response theory: The monomers are linearly coupled to the bath oscillators and the coupling function F_i is specified as

$$F_i=\sum_x g_x^{(i)}q_x, \tag{A8}$$

where the coupling parameters $g_x^{(i)}$ describe the interaction of an excitation at site $|i\rangle$ with mode x of the bath. The more general case of the SB interaction, which includes the effect of finite correlation length and terms that are quadratic in the bath coordinate, has been discussed by Kühn and Sundström,[60] May and co-workers.[78,79]

For a bath of harmonic oscillators, analytic expressions for the bath CF and its Fourier transform can be obtained[57] (we neglect the imaginary part of the Redfield tensor, the so-called Lamb shift, which describes a spectral shift of system transitions due to dephasing):

$$\langle F_i(t)F_i\rangle_{\mathrm{B}} = \tfrac{1}{2}\sum_x g_x^{(i)2}[n(\omega_x)e^{i\omega_x t} + (1+n(\omega_x))e^{-i\omega_x t}], \tag{A9}$$

$$\begin{aligned}\tilde{C}_i(\omega) &= \mathrm{Re}\int_0^\infty dt\langle F_i(t)F_i\rangle_{\mathrm{B}} e^{-i\omega t} \\ &= n(\omega)J_i(\omega) + (1+n(-\omega))J_i(-\omega) \\ &= \begin{cases} n(\omega)J_i(\omega) & \text{if } \omega > 0 \\ (1+n(-\omega))J_i(-\omega) & \text{if } \omega < 0. \end{cases}\end{aligned} \tag{A10}$$

Here, $n(\omega)=1/(e^{\omega/kT}-1)$ is the Bose thermal distribution function, and the spectral density function, $J_i(\omega)$, which entirely describes the parameters of the bath, is defined for each monomer as

$$J_i(\omega) = \frac{\pi}{2}\sum_x g_x^{(i)2}\delta(\omega-\omega_x). \tag{A11}$$

For convenience we assume that the spectral density for both monomers is equivalent. For the calculations in this paper, the spectral density is taken to be of the form

$$J(\omega) = g^2\frac{\omega}{\omega_c}\exp(-\omega/\omega_c), \tag{A12}$$

where ω_c is a cutoff frequency and g^2 is a dimensionless coupling strength parameter.

APPENDIX B: SECULAR APPROXIMATION

Next we employ a secular approximation that is widely accepted in Redfield theory for relaxation processes. We consider only so-called secular terms of the Redfield tensor satisfying

$$|\omega_{\mu\nu} - \omega_{\kappa\lambda}| = 0. \tag{B1}$$

In this case the equations of motion for populations and coherences are decoupled: Populations obey the Pauli master equation (rate equations)

$$\partial_t\rho_{\mu\mu}(t)|_{\mathrm{diss}} = -\Gamma_{\mu\mu}\rho_{\mu\mu}(t) + \sum_{\nu\neq\mu}\gamma_{\mu\nu}\rho_{\nu\nu}(t), \tag{B2}$$

where $\gamma_{\mu\nu}\equiv\gamma_{\mu\leftarrow\nu}$ is the relaxation rate from state ν to state μ and

$$\Gamma_{\mu\mu} = \sum_{\lambda\neq\mu}\gamma_{\lambda\mu}, \tag{B3}$$

while coherences show an exponential decay

$$\partial_t\rho_{\mu\nu}(t)|_{\mathrm{diss}} = -\Gamma_{\mu\nu}\rho_{\mu\nu}(t). \tag{B4}$$

The Redfield tensor reduces to the rate matrices[57]

$$\gamma_{\mu\nu} \equiv R_{\mu\mu\nu\nu} = \Gamma^+_{\nu\mu\mu\nu} + \Gamma^-_{\nu\mu\mu\nu} \quad \text{for } \mu\neq\nu, \tag{B5}$$

describing population relaxation, and

$$\begin{aligned}\Gamma_{\mu\nu} &\equiv -R_{\mu\nu\mu\nu} = -\Gamma^+_{\nu\nu\mu\mu} - \Gamma^-_{\nu\nu\mu\mu} + \sum_\lambda\Gamma^+_{\mu\lambda\lambda\mu} + \sum_\lambda\Gamma^-_{\nu\lambda\lambda\nu} \\ &= \hat{\Gamma}_{\mu\nu} + \tfrac{1}{2}\sum_{\lambda\neq\mu}\gamma_{\lambda\mu} + \tfrac{1}{2}\sum_{\lambda\neq\nu}\gamma_{\lambda\nu},\end{aligned} \tag{B6}$$

describing coherence dephasing. The latter consists of population relaxation rates and so-called pure dephasing,

$$\begin{aligned}\hat{\Gamma}_{\mu\nu} &= -\Gamma^+_{\nu\nu\mu\mu} - \Gamma^-_{\nu\nu\mu\mu} + \Gamma^+_{\nu\nu\nu\nu} + \Gamma^-_{\mu\mu\mu\mu} \\ &= \mathrm{Re}\int_0^\infty dt\langle[\langle\mu|H^{\mathrm{SB}}(t)|\mu\rangle - \langle\nu|H^{\mathrm{SB}}(t)|\nu\rangle] \\ &\quad\times[\langle\mu|H^{\mathrm{SB}}|\mu\rangle - \langle\nu|H^{\mathrm{SB}}|\nu\rangle]\rangle_{\mathrm{B}},\end{aligned} \tag{B7}$$

which is a generalization of the well-known relation between the relaxation times T_1 and T_2. The elements of the transformation matrix which diagonalize the dimer Hamiltonian (5) have a simple form [Eq. (10)], and all rates $\gamma_{\mu\nu}$ and $\Gamma_{\mu\nu}$ are written explicitly in Appendix C.

APPENDIX C: DIMER RELAXATION AND DEPHASING RATES

In this appendix, we give the relaxation and dephasing rates for the dimer. The population relaxation and pure dephasing rates between one-exciton states are

$$\gamma_{\alpha\beta} = 2\sum_i |C_i^\alpha|^2|C_i^\beta|^2\tilde{C}(\omega_{\alpha\beta}) = \sin^2 2\theta\tilde{C}(\omega_{\alpha\beta}),$$
$$\alpha,\beta = 1,2, \tag{C1}$$

$$\hat{\Gamma}_{\alpha\beta} = \sum_i (|C_i^\alpha|^2 - |C_i^\beta|^2)^2\tilde{C}(0) = 2\cos^2 2\theta\tilde{C}(0). \tag{C2}$$

For the spectral density (A12), a zero-frequency limit that determines the pure dephasing rate is $\tilde{C}(0)=g^2kT/\omega_c$. Note that the detailed balance condition (the relation between the downhill, γ_{12}, and uphill, γ_{21}, rates) is satisfied: $\gamma_{12}=e^{\omega_{21}/kT}\gamma_{21}$, i.e., $\gamma_{12}>\gamma_{21}$. Obviously, if there are only two states in the manifold then $\Gamma_{11}=\gamma_{21}$ and $\Gamma_{22}=\gamma_{12}$.

Coherence dephasing rates that appear in the equations of motion [(D1)–(D6)] are defined as follows:

$$\Gamma_{\alpha 0} = \hat{\Gamma}_{\alpha 0} + \tfrac{1}{2}\gamma_{\beta\alpha}, \tag{C3}$$

$$\Gamma_{\alpha\beta} = \hat{\Gamma}_{\alpha\beta} + \tfrac{1}{2}(\gamma_{\alpha\beta} + \gamma_{\beta\alpha}), \tag{C4}$$

$$\Gamma_{\bar{\alpha}\alpha} = \hat{\Gamma}_{\bar{\alpha}\alpha} + \tfrac{1}{2}\gamma_{\beta\alpha}, \tag{C5}$$

$$\Gamma_{\bar{\alpha}0} = \hat{\Gamma}_{\bar{\alpha}0}. \tag{C6}$$

The explicit expressions for pure dephasing rates in the dimer are

$$\hat{\Gamma}_{\alpha 0} = \sum_i |C_i^\alpha|^4\tilde{C}(0) = \left(1 - \tfrac{1}{2}\sin^2 2\theta\right)\tilde{C}(0) \tag{C7}$$

for the coherence connecting one-exciton states with the ground state and

$$\hat{\Gamma}_{\bar{\alpha}0} = \sum_{i>j} |C_{ij}^{\bar{\alpha}}|^2 \Bigg\{ \sum_{i>k} |C_{ik}^{\bar{\alpha}}|^2 + \sum_{i<k} |C_{ki}^{\bar{\alpha}}|^2 + \sum_{j>k} |C_{jk}^{\bar{\alpha}}|^2 + \sum_{j<k} |C_{kj}^{\bar{\alpha}}|^2 \Bigg\} \tilde{C}(0) = 2\tilde{C}(0) \tag{C8}$$

for the two-exciton coherence. Finally, the pure dephasing rate for the one-two-exciton coherence is the same as for the one-exciton coherence (this holds only for the dimer):

$$\hat{\Gamma}_{\bar{\alpha}\alpha} = \hat{\Gamma}_{\alpha 0}. \tag{C9}$$

APPENDIX D: EQUATIONS OF MOTION FOR THE DIMER IN RWA

Introducing the ansatz (22) into the Liouville equation (19) we find the following equations for one-exciton coherence:

$$\partial_t \sigma_{10} = -i(\omega_{10} - \Omega)\sigma_{10} - \Gamma_{10}\sigma_{10} + i\mathbf{E}(t)\{\mu_{10}(\rho_{00} - \rho_{11}) - \mu_{20}\rho_{12}\} + i\mathbf{E}^*(t)\mu_{31}\sigma_{30}, \tag{D1}$$

coherence between two- and one-exciton states:

$$\partial_t \sigma_{31} = -i(\omega_{31} - \Omega)\sigma_{31} - \Gamma_{31}\sigma_{31} + i\mathbf{E}(t)\{\mu_{31}\rho_{11} + \mu_{32}\rho_{21}\} - i\mathbf{E}^*(t)\mu_{10}\sigma_{30}, \tag{D2}$$

two-exciton coherence:

$$\partial_t \sigma_{30} = -i(\omega_{30} - 2\Omega)\sigma_{30} - \Gamma_{30}\sigma_{30} + i\mathbf{E}(t)\{\mu_{31}\sigma_{10} + \mu_{32}\sigma_{20} - \mu_{10}\sigma_{31} - \mu_{20}\sigma_{32}\}, \tag{D3}$$

one-exciton population:

$$\partial_t \rho_{11} = -\Gamma_{11}\rho_{11} + \gamma_{12}\rho_{22} + i\mathbf{E}(t)\{\mu_{10}\sigma_{01} - \mu_{31}\sigma_{13}\} + i\mathbf{E}^*(t)\{\mu_{31}\sigma_{31} - \mu_{10}\sigma_{10}\}, \tag{D4}$$

intraband (one-exciton manifold) coherence:

$$\partial_t \rho_{12} = -i\omega_{12}\rho_{12} - \Gamma_{12}\rho_{12} + i\mathbf{E}(t)\{\mu_{10}\sigma_{02} - \mu_{32}\sigma_{13}\} + i\mathbf{E}^*(t)\{\mu_{31}\sigma_{32} - \mu_{20}\sigma_{10}\}, \tag{D5}$$

and ground-state population:

$$\partial_t \rho_{00} = -i\mathbf{E}(t)\{\mu_{10}\sigma_{01} + \mu_{20}\sigma_{02}\} + i\mathbf{E}^*(t)\{\mu_{10}\sigma_{10} + \mu_{20}\sigma_{20}\}. \tag{D6}$$

Note that we use indices 0 and 3 for the ground state $|g\rangle$ and two-exciton state $|\bar{\alpha}\rangle$, respectively. The equations for the RDM elements involving state $\alpha=2$ (namely, σ_{20}, σ_{32}, and ρ_{22}) are obtained by the substitution $1 \leftrightarrow 2$ in the corresponding equations involving state $\alpha=1$.

[1] P. Hamm, M. Lim, and R. M. Hochstrasser, J. Phys. Chem. B **102**, 6123 (1998).
[2] P. Hamm, M. Lim, W. F. DeGrado, and R. M. Hochstrasser, J. Phys. Chem. A **103**, 10049 (1999).
[3] M. C. Asplund, M. T. Zanni, and R. M. Hochstrasser, Proc. Natl. Acad. Sci. U.S.A. **97**, 8219 (2000).
[4] N.-H. Ge, M. T. Zanni, and R. M. Hochstrasser, J. Phys. Chem. A **106**, 962 (2002).
[5] C. Fang, J. Wang, A. K. Charnley, W. Barber-Armstrong, A. B. Smith III, S. M. Decatur, and R. M. Hochstrasser, Chem. Phys. Lett. **382**, 586 (2003).
[6] M. Khalil and A. Tokmakoff, Chem. Phys. **266**, 213 (2001).
[7] N. Demirdoven, M. Khalil, and A. Tokmakoff, Phys. Rev. Lett. **89**, 237401 (2002).
[8] M. Khalil, N. Demirdoven, and A. Tokmakoff, J. Phys. Chem. A **107**, 5258 (2003).
[9] M. Khalil, N. Demirdoven, and A. Tokmakoff, Phys. Rev. Lett. **90**, 047401 (2003).
[10] Y. Tanimura and S. Mukamel, J. Chem. Phys. **99**, 9496 (1993).
[11] S. Saito and I. Ohmine, Phys. Rev. Lett. **88**, 207401 (2002).
[12] L. J. Kaufman, J. Y. Heo, L. D. Ziegler, and G. R. Fleming, Phys. Rev. Lett. **88**, 207402 (2002).
[13] K. J. Kubarych, C. J. Milne, S. Lin, V. Astinov, and R. J. D. Miller, J. Chem. Phys. **116**, 2016 (2002).
[14] K. J. Kubarych, C. J. Milne, and R. J. D. Miller, Int. Rev. Phys. Chem. **22**, 437 (2003).
[15] S. M. G. Faeder, A. W. Albrecht, J. D. Hybl, B. L. Landin, B. Rajaram, and D. M. Jonas, J. Opt. Soc. Am. B **15**, 2338 (1998).
[16] J. D. Hybl, A. W. Albrecht, S. M. G. Faeder, and D. M. Jonas, Chem. Phys. Lett. **297**, 307 (1998).
[17] J. D. Hybl, A. A. Ferro, and D. M. Jonas, J. Chem. Phys. **115**, 6606 (2001).
[18] J. D. Hybl, A. Yu, D. A. Farrow, and D. M. Jonas, J. Phys. Chem. A **106**, 7651 (2002).
[19] N. Belabas and M. Joffre, Opt. Lett. **27**, 2043 (2002).
[20] M. L. Cowan, J. P. Ogilvie, and R. J. D. Miller, Chem. Phys. Lett. **386**, 184 (2004).
[21] T. Brixner, I. V. Stiopkin, and G. R. Fleming, Opt. Lett. **29**, 884 (2004).
[22] T. Brixner, T. Mančal, I. V. Stiopkin, and G. R. Fleming, J. Chem. Phys. **121**, 4221 (2004).
[23] T. Brixner, J. Stenger, H. M. Vaswani, M. Cho, R. E. Blankenship, and G. R. Fleming, Nature (London) **434**, 625 (2005).
[24] A. Takmakoff, J. Phys. Chem. A **104**, 4247 (2000).
[25] S. Mukamel, Annu. Rev. Phys. Chem. **51**, 691 (2000).
[26] S. Woutersen and P. Hamm, J. Phys.: Condens. Matter **14**, R1035 (2002).
[27] J. Sung and R. J. Silbey, J. Chem. Phys. **115**, 9266 (2001).
[28] J. Sung and R. J. Silbey, J. Chem. Phys. **118**, 2443 (2003).
[29] M. Cho, H. M. Vaswani, T. Brixner, J. Stenger, and G. R. Fleming, J. Phys. Chem. B **109**, 10542 (2005).
[30] R. E. Fenna and B. W. Matthews, Nature (London) **258**, 573 (1975).
[31] Y.-F. Li, W. Zhou, R. E. Blankenship, and J. P. Allen, J. Mol. Biol. **271**, 456 (1997).
[32] M. Yang and G. R. Fleming, J. Chem. Phys. **110**, 2983 (1999).
[33] B. S. Prall, D. Y. Parkinson, G. R. Fleming, M. Yang, and N. Ishikawa, J. Chem. Phys. **120**, 2537 (2004).
[34] M. Cho and G. R. Fleming, J. Chem. Phys. **123**, 114506 (2005).
[35] S. Mukamel, *Principles of Nonlinear Optical Spectroscopy* (Oxford University Press, New York, 1995).
[36] T. Mančal, A. V. Pisliakov, and G. R. Fleming, J. Chem. Phys. **124**, 234504 (2006).
[37] M. H. Vos, J. C. Lambry, S. J. Robles, D. C. Youvan, J. Breton, and J. L. Martin, Proc. Natl. Acad. Sci. U.S.A. **88**, 8885 (1991).
[38] M. H. Vos, F. Rappaport, J. C. Lambry, J. Breton, and J. L. Martin, Nature (London) **363**, 320 (1993).
[39] M. Chachisvilis, T. Pullerits, M. R. Jones, C. N. Hunter, and V. Sundström, Chem. Phys. Lett. **224**, 345 (1994).
[40] R. J. Stanley and S. G. Boxer, J. Phys. Chem. **99**, 859 (1995).
[41] P. J. Reid, C. Silva, P. F. Barbara, L. Karki, and J. T. Hupp, J. Phys. Chem. **99**, 2609 (1995).
[42] S. Engleitner, M. Seel, and W. Zinth, J. Phys. Chem. **103**, 3013 (1999).
[43] I. Rubtsov and K. Yoshihara, in *Femtochemistry*, edited by F. C. De-Schryver, S. D. Feyter, and G. Schweiteret (Wiley, Berlin, 2001), pp. 367–380.
[44] C. Zimmermann, F. Willig, S. Ramakrishna, B. Burfeindt, B. Pettinger, R. Eichberger, and W. Storck, J. Phys. Chem. B **105**, 9245 (2001).
[45] J. Stenger, D. Madsen, J. Dreyer, E. T. J. Nibbering, P. Hamm, and T. Elsaesser, J. Phys. Chem. A **105**, 2929 (2001).
[46] D. H. Son, P. Kambhampati, T. W. Kee, and P. F. Barbara, J. Phys. Chem. A **106**, 4591 (2002).
[47] N. Mataga, H. Chosrowjan, Y. Shibata, Y. Imamoto, M. Kataoka, and F. Tokunaga, Chem. Phys. Lett. **352**, 220 (2002).
[48] J. Jean, R. Friesner, and G. Fleming, J. Chem. Phys. **96**, 5827 (1992).
[49] J. Tang and S. H. Lin, Chem. Phys. Lett. **254**, 6 (1996).
[50] A. Lucke, C. H. Mak, R. Egger, J. Ankerhold, J. Stockburger, and H. Grabert, J. Chem. Phys. **107**, 8397 (1997).
[51] J. Casado-Pascual, C. Denk, M. Morillo, and R. I. Cukier, J. Chem. Phys. **113**, 11176 (2000).

[52] D. Egorova, A. Kühl, and W. Domcke, Chem. Phys. **268**, 105 (2001).
[53] T. O. Cheche and S. H. Lin, Phys. Rev. E **64**, 061103 (2001).
[54] A. V. Pisliakov, M. F. Gelin, and W. Domcke, J. Phys. Chem. A **107**, 2657 (2003).
[55] H. van Amerongen, L. Valkunas, and R. van Grondelle, *Photosynthetic Excitons* (World Scientific, Singapore, 2000).
[56] L. Seidner, G. Stock, and W. Domcke, J. Chem. Phys. **103**, 3998 (1995).
[57] K. Blum, *Density Matrix Theory and Applications* (Plenum, New York, 1981).
[58] M. H. Vos, M. R. Jones, and J.-L. Martin, Chem. Phys. **233**, 179 (1998).
[59] J. M. Jean and G. R. Fleming, J. Chem. Phys. **103**, 2092 (1995).
[60] O. Kühn and V. Sundström, J. Chem. Phys. **107**, 4154 (1997).
[61] T. Renger and V. May, J. Phys. Chem. A **102**, 4381 (1998).
[62] M. Yang and G. R. Fleming, Chem. Phys. **275**, 355 (2002).
[63] M. Yang, A. Damjanovic, H. M. Vaswani, and G. R. Fleming, Biophys. J. **85**, 140 (2003).
[64] O. Kühn, T. Renger, and V. May, Chem. Phys. **204**, 99 (1996).
[65] V. May and O. Kühn, *Charge and Energy Transfer Dynamics in Molecular Dynamics* (Wiley-VCH, Berlin, 2002).
[66] A. G. Redfield, Adv. Magn. Reson. **1**, 1 (1965).
[67] D. M. Jonas, Annu. Rev. Phys. Chem. **54**, 425 (2003).
[68] W. H. Press, B. P. Flannery, S. A. Teukolsky, and W. T. Vetterling, *Numerical Recipes* (Cambridge University Press, Cambridge, 1986).
[69] A. A. Ferro, J. D. Hybl, and D. M. Jonas, J. Chem. Phys. **114**, 4649 (2001).
[70] M. Khalil, N. Demirdoven, and A. Tokmakoff, J. Chem. Phys. **121**, 362 (2004).
[71] A. Piryatinski, V. Chernyak, and S. Mukamel, Chem. Phys. **266**, 285 (2001).
[72] C. Scheurer and S. Mukamel, J. Chem. Phys. **115**, 4989 (2001).
[73] M. Yang, K. Ohta, and G. R. Fleming, J. Chem. Phys. **110**, 10243 (1999).
[74] M. Yang and G. R. Fleming, J. Chem. Phys. **113**, 2823 (2000).
[75] R. Venkatramani and S. Mukamel, J. Chem. Phys. **117**, 11089 (2002).
[76] S. I. E. Vulto, M. A. de Baat, R. J. W. Louwe, H. P. Permentier, T. Neef, M. Miller, H. van Amerongen, and T. J. Aartsma, J. Phys. Chem. B **102**, 9577 (1999).
[77] R. Agarwal, M. Yang, Q. H. Xu, and G. R. Fleming, J. Chem. Phys. **110**, 10243 (1999).
[78] T. Renger and V. May, J. Phys. Chem. B **101**, 7232 (1997).
[79] T. Renger, O. Kühn, and V. May, Phys. Rep. **343**, 137 (2001).